

**MARES:****A macroscopic model for the Radar Echo Telescope  
Contribution to ICRC 2023**

---

**Enrique Huesca Santiago<sup>a,\*</sup> and Krijn de Vries<sup>a</sup> for the RET collaboration***<sup>a</sup>Inter-University Institute for High Energies, Vrije Universiteit Brussel,  
Pleinlaan 2, 1050 Elsene, Belgium**E-mail: [e.huescasantiago@gmail.com](mailto:e.huescasantiago@gmail.com), [krijndevries@gmail.com](mailto:krijndevries@gmail.com)*

Upon interaction in a dense medium like polar ice, a high-energy neutrino will deposit its energy abruptly, producing a short-lived electron plasma. The Radar Echo Telescope (RET) collaboration aims to utilize the radar technique to probe this plasma and, thus, detect neutrinos in the PeV to EeV energy range. This work presents the Macroscopic Approach to the Radar Echo Scatter (MARES) model. MARES is based on a macroscopic, semi-analytical approach and includes all the known relevant physics that will affect the radar signal. Here we show how MARES is used to investigate the effect that the ice temperature, via the free electron lifetime, might have on the radar scatter signal.

38th International Cosmic Ray Conference (ICRC2023)  
26 July - 3 August, 2023  
Nagoya, Japan



---

\*Speaker

## 1. Introduction

The Radar Echo Telescope (RET) collaboration aims to detect the interaction of high-energy (HE) cosmic neutrinos in polar ice. So far, the cosmic neutrino flux has been characterised in the TeV - PeV region by the IceCube neutrino observatory [1]. Beyond 10 PeV, the steeply falling flux suppresses the likelihood of neutrino detection. However, cosmic neutrinos are expected to be produced in the interactions of ultra-high-energy cosmic-rays with the cosmic microwave background photons [2]. Based on the measured flux of ultra-high-energy cosmic rays at Earth up to the 100 EeV range [3], cosmic neutrinos reaching the Earth with EeV energies are expected. The RET collaboration hopes to utilise the radar echo technique to measure the cosmic neutrino flux in the PeV to EeV range.

The radar echo technique involves instrumenting a large volume of ice with a radar system, consisting of, at least, one radio transmitter and several radio receiver antennas. When a high-energy neutrino interacts in the ice, it will initiate a particle cascade, which extends for  $O(10\text{ m})$  in the ice. The particle cascade will, in turn, deposit the bulk of its energy in the ice in a short timescale, leaving in its wake a trail of ionised ice and free electrons. These low-energy electrons form a plasma that is capable of scattering the transmitter's radio waves, which will be recorded at the receivers. At energies over 10 PeV, the number density of particles in the cascade and the subsequent plasma have been estimated to be high enough to make its detection feasible [4, 5]. Radio waves hold an important advantage over optical-based detection methods, as the radio attenuation length in ice is  $O(1\text{ km})$ , as opposed to the attenuation length of  $O(100\text{ m})$  of optical light. This makes a more sparse detector configuration possible, therefore increasing the exposure to the high-energy cosmic neutrino flux.

In order to study the viability of the radar echo technique as an in-ice neutrino telescope, we need a deep understanding of the physics behind the radar scatter off a plasma induced by a particle cascade in ice. So far, the modelling of the radar scatter was done with RadioScatter [6], a particle-level simulation of ionization deposits generated by MonteCarlo (MC) techniques.

In this work we present the basis of MARES, a macroscopic model of the radar echo scatter. MARES is a semi-analytical model that relies on the known parametrisation of the particle cascades to compute the expected signal from a radar scatter event. Our focus here is to outline the procedure to discretise the extended plasma while maintaining the accuracy of the scatter. Furthermore, as will be outlined in a forthcoming paper, other effects such as wave polarisation, medium attenuation, etc. are also taken into account by the model and included in the simulation of the final signal. In addition, as a non-MonteCarlo model, MARES simulations presents a deterministic nature; the same result is always expected using the same set of input parameters. As an example of this, we show-case here the impact that the ionisation electron lifetime has on the final signal strength and structure.

The Radar Echo Telescope's ongoing experimental efforts at Summit Station, Greenland, called the Radar Echo Telescope for cosmic rays (RET-CR), are presented in detail in [7] and in [8] in these proceedings. The Radar Echo Telescope for Neutrinos (RET-N) outlook and preliminary design can be found in [9] in these proceedings.

## 2. The basic principle of the radar scatter theory

For any point within the region illuminated by the transmitter, there is an incident electric field

$$|E_{in}| = \sqrt{2Z_{ice}I_{in}} = \sqrt{2Z_{ice} \left( \frac{P_T G_T}{4\pi R_T^2} \right)}, \quad (1)$$

where  $P_T$ ,  $G_T$  and  $R_T$  are the power, directional gain and distance to the transmitter; and  $I_{in}$  is the incident irradiance from the transmitter and  $Z_{ice}$  the medium (for this case, ice) impedance.

Any scatterer, will act as a secondary source of radio waves, and the far-field ratio between the incident and scattered electric field amplitudes is the radar cross section, RCS or  $\sigma$ ,

$$\sigma = \lim_{r \rightarrow \infty} 4\pi r^2 \frac{|E_{sc}|^2}{|E_{in}|^2} \quad (2)$$

A receiver of effective area  $A_R$  at a distance  $R_R$  (assumed large) will measure a power  $P_R$ ,

$$P_R = I_{sc} A_R = \frac{|E_{sc}|^2}{2Z_{ice}} A_R = \frac{1}{2Z_{ice}} \left( \frac{|E_{in}|^2}{4\pi R_R^2} \sigma \right) A_R. \quad (3)$$

Putting Eq. 1 and Eq. 3 together for a single scatterer, we arrive at the radar range equation:

$$P_R = \frac{P_T G_T A_R}{(4\pi R_T R_R)^2} \sigma. \quad (4)$$

If  $N$  separate scatters arrive at the receiver simultaneously, the power measured by the antenna will be determined by the interference of their electric fields:

$$P_{RX}(t) = \frac{P_T G_T A_R}{(4\pi)^2} \left| \sum_{i=1}^N \frac{\sqrt{\sigma_i}}{R_{T,i} R_{R,i}} \cdot e^{i\phi_i} \right|^2. \quad (5)$$

In this case, knowing the radar scattering cross section  $\sigma_i$  of the  $N$  scatterers is not enough to compute the total signal, we also need to know their respective space-time phase  $\phi_i$ , which is computed from the cascade's relative position and direction with respect to the transmitter and receiver antennas. Exact definitions of both terms are given in Sec. 3.1. Examining Eq. 5 closely, if  $m$  scattering sources of similar  $\sigma$  are coherent, this is, if the difference between their phases is negligible  $\phi_1 \approx \phi_2 \approx \dots \phi_m = \phi$ , the power received will scale like the square of the number of sources:

$$P_{R,i} \propto |\vec{E}_{R,i}(R_i, t)|^2 = N_m^2 P_{R,m} \quad (6)$$

The criterion for coherence can be safely taken as any typical distance ( $l$ ) smaller than a wavelength,  $l < \lambda$  [10]. For a typical transmitter frequency  $f_T < 100$  MHz,  $\lambda_{ice} \simeq 200$  cm, and  $l$  can take values  $\leq 10$  cm while maintaining coherence, decreasing to  $l_{min} \leq 1$  cm,  $f_T = 1$  GHz. Any discrete collection of scatters fulfilling the coherence criterion, i.e., within the cm scale, can be considered as a single source. Therefore, the 1-10 cm scale is the smallest scale that we need to consider in the radar scatter, well within the macroscopic realm.

### 3. MARES: From the cascade to the signal

A neutrino interaction in the ice initiates a particle cascade of  $L \sim \mathcal{O}(10 \text{ m})$ ,  $r_{\text{moliere}} = 7 \text{ cm}$ . The secondary particles from the cascade will deposit their energy in the ice, ionising the medium and freeing electrons. We assume that all energy deposited in the ice will be used for electron ionisation, producing  $\mathcal{O}(10^{13} e^-)$  per PeV. MARES uses a NKG parametrisation for the cascade [5] [11], and the resulting plasma is depicted in Fig. 1.

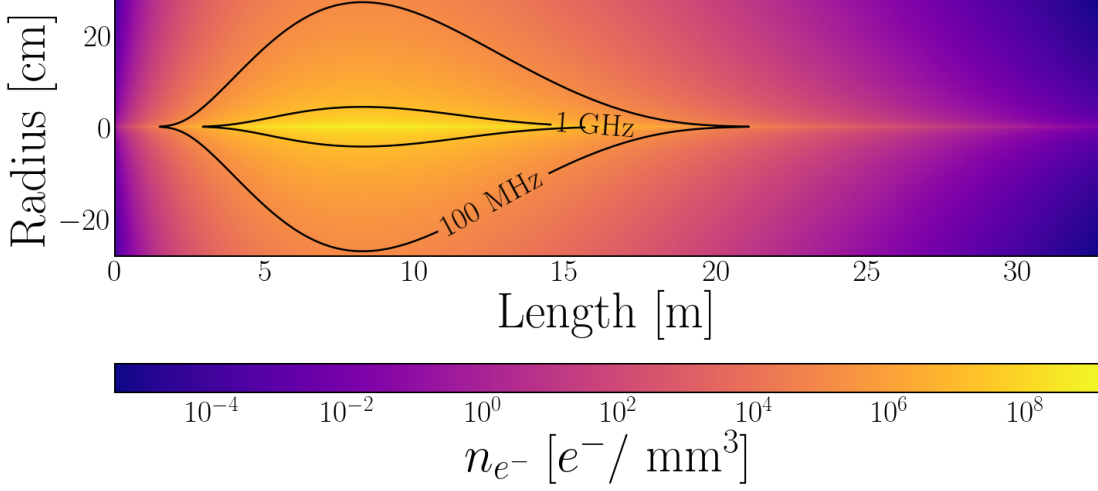


**Figure 1:** The cascade density profile  $n_e$  of a  $10^7 \text{ GeV}$  primary. The density and plasma frequency  $\nu_p$  scale with the energy of the cascade's primary,  $E_p$ . Curves of constant plasma frequency (and density) have been added for reference.

Instead of attempting to track the individual fields of the  $\mathcal{O}(10^{14})$  electrons, we can take advantage of the coherence condition (Eq. 6) and discretize the cascade into  $M$  volumes where the  $N_{e,i}$ ;  $i = 1, \dots, M$  electrons scatter coherently. First, as seen in Fig. 1, the electron distribution is radially symmetric, which makes our choice of volume a semi-cylindrical shell of length 1 cm and thickness 1 mm, all of them placed concentrically along the length axis. This way, the cascade is reduced to  $\approx 10^6$  scattering volumes where the electron density can be taken as constant though each volume. Second, it is important to notice the small scale of the radial dimension,  $R_{\text{max}} \sim \lambda_{\text{ice}}$ , where most of the electrons are around the core,  $R_{\text{moliere}} \leq \lambda$ . This means that the coherence condition may be extended to all electrons throughout the plasma's radial dimension at any given length. Then, we perform a second integration where we add up the semi-cylindrical layers into segments, still placed along the length axis. The cascade is further reduced down to  $10^4$  separate scatterers of 1 cm. Finally, having established our segments as the scatterers of this model, we can turn to Eq. 5 to simulate the radar scatter of the cascade by computing the  $10^4$  segments numerically.

#### 3.1 The radar cross section and phase of a single segment

Eq. 5 requires the radar scattering cross section and the phase of each segment. The time-independent radar cross section of a segment,  $\sigma_{sc}$ , containing  $N_{e,i}$  electrons, can be written in terms of the radar cross section for a single electron  $\sigma_e$ [11]:

$$\sigma_{sc,i} = N_{e,i}^2 \sigma_e = N_{e,i}^2 \cdot (\sigma_{Th} (\omega_T^2 W)^2 \mathcal{T} G_{Hz}). \quad (7)$$

The effective electron RCS  $\sigma_e$  is composed not just of the Thompson scattering cross section  $\sigma_{Th}$ , but captures important physics effects: the damping factor  $(\omega_T^2 W)^2 \leq 10^{-10}$  corrects the decrease in perceived RCS due to the collisions of the electron with the ice medium,  $G_{Hz}$  is the Hertzian gain factor, to reflect that electrons re-scatter like infinitesimal dipoles, not isotropically, and  $\mathcal{T} \sim 1$  is the transparency correction, that represents the losses of the field strength due to the screening of the rest of the plasma. The full derivation of the radar cross section for a scattering segment  $\sigma_{sc}$ , where these concepts were introduced and discussed in detail, can be found in [11].

However, the description of the radar scatter has considered of a series of static charges so far. In reality, the ice lattice is ionised only after the relativistic propagation of the cascade front, which introduces a time-dependent relationship between the position (and therefore, its distances  $R_{T,i}$ ,  $R_{R,i}$ ) and the production time of a segment ( $t_{0,i}$ ). MARES models the evolution of the cascade by evaluating the instantaneous fields (Eq. 5) multiple times over the lifetime of the cascade (see next section for details), using segments with time-independent position, and time-dependent phases and radar cross section (see Eq 8).

The time-dependent segment phases are described as  $\phi_i = kR_i - \omega t_R + \psi_i$ ; that includes the total distance travelled,  $R_i = R_{T,i} + R_{R,i}$ ; the time of arrival at the receiver,  $t_R$  (which needs to account for retardation effects,  $t_R = t_{sc} + R_{R,i}/c_{ice}$ ); and any individual phase that each segment might have,  $\psi_i$ . The time-dependence of the phases of the different segments determines the interference of the electric fields and captures the crucial geometrical and relativistic effects of the scatter. This allows MARES to simulate accurate time-domain waveforms of the radar scatter, at the cost of increased the computational complexity.

#### 4. The effect of the plasma lifetime

The free electron decay rate  $f_r$ , and therefore the free electron lifetime  $\tau = f_r^{-1}$ , are primarily a function of the ice's temperature [12]. Based on reported polar ice temperatures [13] [14], we take typical ice values of  $T_{SP} = -50$  C for South Pole and  $T_G = -30$  C for Greenland. This translates to  $\tau_{SP} \approx 20$  ns,  $f_{r,SP} \approx 5 \cdot 10^7$  Hz and  $\tau_G \approx 2$  ns,  $f_{r,G} \approx 5 \cdot 10^8$  Hz. Since the ice temperature depends on site and depth, in the following we consider a range of  $\tau \in [1, 50]$  ns.

The  $f_r$  is much smaller than the collision frequency  $f_c \sim \mathcal{O}(10-100)$  THz, which can only be explained if we assume the collisions to be (quasi-)elastic. On the other hand,  $f_r \sim f_{TX} \in [10$  MHz, 1 GHz] where  $f_{TX}$  is the frequency of transmitter. Since the ionisation electrons are only able to scatter in the free state, the complete microscopic picture of the scatter is that of the sudden appearance of a free ionisation electron, scattering weakly as it is damped by collisions, and re-attaching itself after being able to complete approximately one full oscillation, as shown already by Radioscatter [6]. This means that there is no complete description of the radar scatter in ice without accounting for the effect of the finite electron lifetime. This is represented in MARES by the time-dependent radar cross section:

$$\sigma_{sc,i}(t) = \sigma_{sc,i} e^{-\frac{t}{\tau}} \Theta(t - t_0) = \sigma_{Th} N_e^2 (\omega^2 W)^2 G_{Hz} \mathcal{T} \cdot e^{-\frac{(t-t_0)}{\tau}} \Theta(t - t_0). \quad (8)$$

The Heaviside step function  $\Theta$  cancels the contribution for times prior at the production time  $t_0$ , while  $e^{-\frac{(t-t_0)}{\tau}}$  captures the re-trapping of the free electrons within the segment.

On the macroscopic level,  $\tau$  determines the instantaneous total of free particles that scatter at any given point in time,  $N_{e^-,ion}$ . As stated before, the total coherent power scales with  $N_e^2$ ; thus even a small change in  $\tau$  has a large impact in the final signal. A direct way to consider this is by investigating the number of free charges available to scatter at any instant in time during the cascade development:

$$N_{e^-,ion}(E_p, t, \tau) = N(E_p, t \cdot c \cdot \rho_{ice}) \otimes e^{-\frac{t}{\tau}} = \int_0^t N(E_p, t') e^{-\frac{(t-t')}{\tau}} dt', \quad (9)$$

which, for our range of  $\tau$  of interest, is shown in Fig. 2.

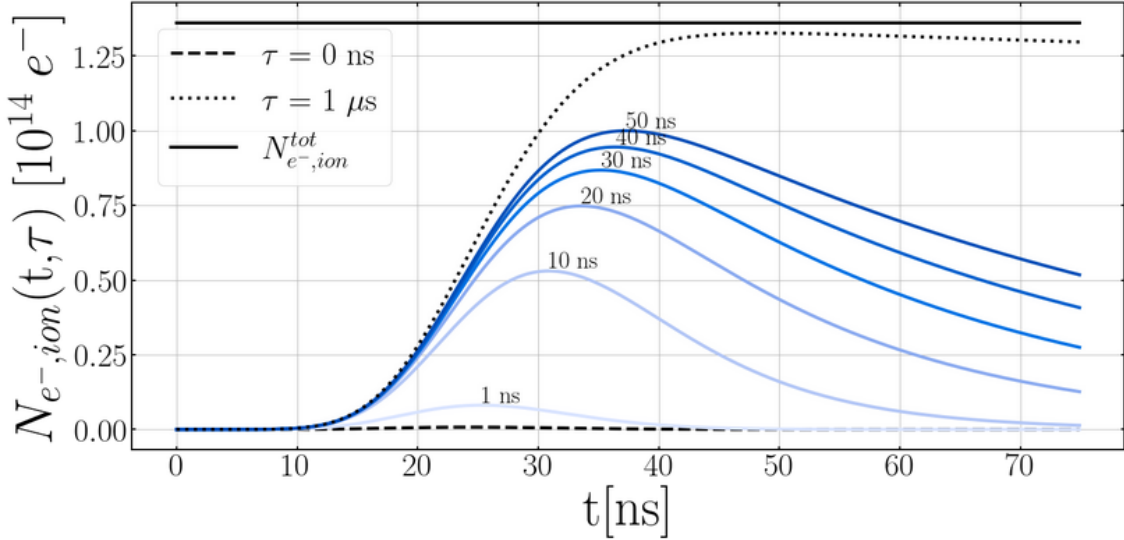


**Figure 2:** The free (ionisation) electron number as function of time for a  $E_p = 10^7$  GeV cascade, with  $t = 0$  being the interaction time. The dashed line ( $\tau = 0$ ) represents the ionization front of the cascade moving through the ice, but you effectively have no scattering from free electrons. The straight, top line is total amount of electrons ionised by the cascade front. As  $\tau$  increases, we expect the peak of the distribution to approach the upper limit, as represented by the unrealistic  $\tau = 1 \mu s$  (dotted line).

To understand Fig. 2 better, we have to visualise the cascade ionisation front leaving the free electron trail in its wake. Because of the free electron lifetime, the characteristic size of the cascade trail is  $l = \tau \cdot c$  and its equivalent radar cross section is determined by  $N_{e^-,ion}$ . By increasing  $\tau$ , the size of the trail increases and more free electrons are scattering at a single instant in time, therefore increasing  $N_{e^-,ion}$ . What is more, increasing  $\tau$  reduces the decay rate  $e^{-\frac{t}{\tau}}$ , increasing the length of the electron distribution tails as seen in in Fig. 2. A very interesting transition seems to happen around  $\tau = 30$  ns, where the growth rate of the distribution peak with  $\tau$  plateaus. This can be explained because at  $\tau = 30$  ns the trail is  $\sim 6$  m long, which is the roughly the size of the cascade.

This means that for  $\tau > 30$  ns the bulk of the cascade electrons are scattering instantaneously. It is important to keep in mind that, given the size of the trail, the scatter of the electron bulk will not be fully coherent unless the transmitter uses a very low frequency. Therefore, the lines in Fig 2 do not show the full picture of the scatter, and it is still of interest to look at the time-domain waveforms (Fig 3).

In Fig. 3, we show the shape of the simulated waveforms by the MARES code of the radar scatter of a 10 PeV cascade in ice at different lifetimes. It is evident that with increasing electron lifetime, the strength and length of the scattered signal increases, but also how its structure is highly suppressed at lifetimes  $\leq 30$  ns. At lifetimes longer than  $\tau = 30$  ns, the peak amplitude becomes constant as the full ionisation profile is visible at once, and the free electron decay becomes apparent in the waveform.

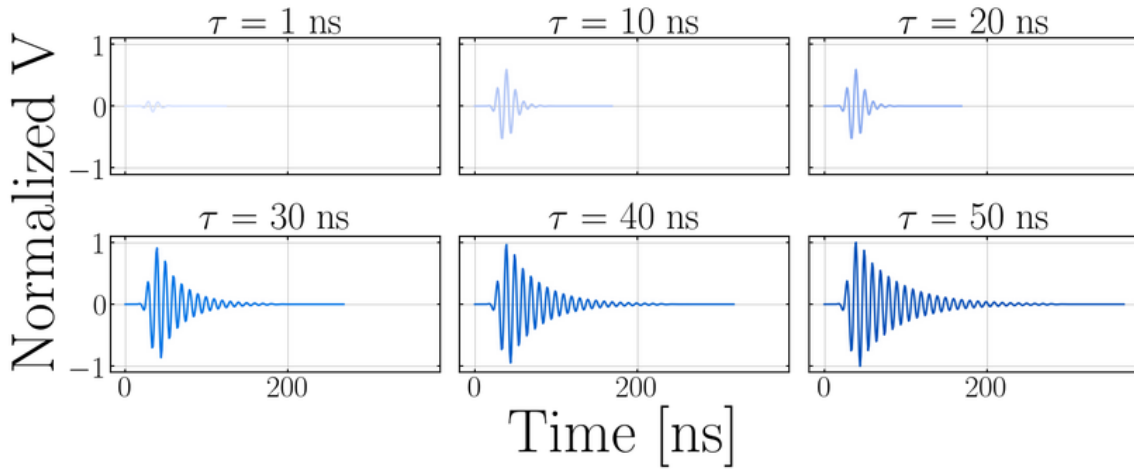


**Figure 3:** Voltage time traces produced from the MARES code, while all the other free model parameters have been kept constant. All the waveforms have been normalised to the highest value (the peak of the  $\tau = 50$  ns trace) for comparison purposes.

## 5. Conclusions

The radar echo technique for the detection of neutrino interactions in polar ice is a promising idea. For the design studies of a future radar telescope and for the characterisation of the properties of the signals that we expect to receive, a deep understanding of the underlying physics is required. That requires a complete model of the scatter of the radio waves off a plasma in ice. MARES is a semi-analytical, non-MonteCarlo model that collects all relevant physics into a single computation. As a macroscopic model, MARES uses the criterion of coherence to integrate all charges under the scale size of 1 – 10 cm without losing accuracy. The investigation of the effect of the variables of the MARES model into the simulated waveforms is underway, and the free electron lifetime, estimated by the ice temperature, is presented here as an example.

## 6. Acknowledgements

RET is funded in part by the National Science Foundation under grant numbers 2012980, 2012989, and 2306424, and the Office of Polar Programs, the Flemish Foundation for Scientific Research FWO-G085820N, the European Research Council under the European Unions Horizon 2020 research and innovation programme (grant agreement No 805486), the Belgian Funds for Scientific Research (FRS-FNRS), IOP, the IceCube EPSCoR Initiative, and the John D. and Catherine T. MacArthur Foundation.

## References

- [1] ICECUBE collaboration, *Evidence for high-energy extraterrestrial neutrinos at the icecube detector*, *Science* **342** (2013) 1242856.
- [2] G. Beresinsky, V.S. and Zatsepin, *Cosmic rays at ultra high energies (neutrino?)*, *Phys. Lett. B* **28** (1969) 423.
- [3] I. Valino et al., *The flux of ultra-high energy cosmic rays after ten years of operation of the Pierre Auger Observatory*, in *Proc. 34 ICRC, The Hauge, The Netherlands, 2015*, DOI.
- [4] M. Chiba et al., *Radar for detection of ultra-high-energy neutrinos reacting in a rock salt dome*, *Nucl. Instrum. Methods. Phys. Res. A* **662** (2012) 222.
- [5] K.D. de Vries, K. Hanson and T. Meures, *On the feasibility of radar detection of high-energy neutrino-induced showers in ice*, *Astropart. Phys.* **60** (2015) 25.
- [6] S. Prohira and D. Besson, *Particle-level model for radar based detection of high-energy neutrino cascades*, *Nucl. Instrum. Methods. Phys. Res. A* **922** (2019) 161.
- [7] RADAR ECHO TELESCOPE collaboration, *The radar echo telescope for cosmic rays: Pathfinder experiment for a next-generation neutrino observatory*, *Phys. Rev. D* **104** (2021) 102006.
- [8] R.S. Stanley et al., *The Radar Echo Telescope for Cosmic Rays*, in *Proc. 38 ICRC, Nagoya, Japan*, no. 474, 2023.
- [9] D. Frikken et al., *The Radar Echo Telescope for Neutrinos*, in *Proc. 38 ICRC, Nagoya, Japan*, no. 1135, 2023.
- [10] G. Rybicki and A.P. Lightman, *Radiative process in astrophysics*, Wiley, 2 ed. (2004).
- [11] E. Huesca Santiago et al., *A macroscopic model of radar detection for the Radar Echo Telescope*, in *9th International Workshop on Acoustic and Radio EeV Neutrino Detection Activities*, 2022.
- [12] M.P. De Haas et al., *Nanosecond time-resolved conductivity studies of pulse-ionized ice. 1. The mobility and trapping of conduction-band electrons in water and deuterium oxide ice*, *J. Phys. Chem.* **87** (1983) 4089.
- [13] P. Buford Price et al., *Temperature profile for glacial ice at the south pole: Implications for life in a nearby subglacial lake*, *PNAS U.S.A.* **99** (2002) 7844.
- [14] J.A. MacGregor et al., *Radar attenuation and temperature within the greenland ice sheet*, *J. Geophys. Res. Earth. Surf.* **120** (2015) 983.

**Full Authors List: The Radar Echo Telescope Collaboration**

P. Allison<sup>1</sup>, J. Beatty<sup>1</sup>, D. Besson<sup>2</sup>, A. Connolly<sup>1</sup>, A. Cummings<sup>3</sup>, C. Deaconu<sup>4</sup>, S. De Kockere<sup>5</sup>, K.D. de Vries<sup>5</sup>, D. Frikken<sup>1</sup>, C. Hast<sup>6</sup>, E. Huesca Santiago<sup>5</sup>, C.-Y. Kuo<sup>7</sup>, A. Kyriacou<sup>2</sup>, U.A. Latif<sup>5</sup>, V. Lukic<sup>5</sup>, K. Mulrey<sup>8</sup>, J. Nam<sup>7</sup>, K. Nivedita<sup>8</sup>, A. Nozdrina<sup>2</sup>, E. Oberla<sup>4</sup>, S. Prohira<sup>2</sup>, J.P. Ralston<sup>2</sup>, M.F.H. Seikh<sup>2</sup>, R.S. Stanley<sup>5</sup>, S. Toscano<sup>9</sup>, D. Van den Broeck<sup>5</sup>, N. van Eijndhoven<sup>5</sup>, and S. Wissel<sup>3</sup>

<sup>1</sup>Department of Physics, Center for Cosmology and AstroParticle Physics (CCAPP), The Ohio State University, Columbus, OH, USA

<sup>2</sup>University of Kansas, Lawrence, KS, USA

<sup>3</sup>Departments of Physics and Astronomy & Astrophysics, Institute for Gravitation and the Cosmos, Pennsylvania State University, University Park, PA, USA

<sup>4</sup>Astronomy & Astrophysics, Kavli Institute for Cosmological Physics, University of Chicago, Chicago, IL, USA

<sup>5</sup>Interuniversity Institute for High Energies, Vrije Universiteit Brussel, Brussel, Belgium

<sup>6</sup>SLAC National Accelerator Laboratory, Menlo Park, CA, USA

<sup>7</sup>National Taiwan University, Taipei, Taiwan

<sup>8</sup>Department of Astrophysics/IMAPP, Radboud University Nijmegen, P.O. Box 9010, 6500 GL Nijmegen, The Netherlands

<sup>9</sup>Interuniversity Institute for High Energies, Université Libre de Bruxelles, Brussels, Belgium